Information Technology Laboratory

**US Army Corps
of Engineers**®
Engineer Research and
Development Center

Innovations for Navigation Projects Research Program

Analysis of the Added Mass of a Barge in Restricted Waters

Phase 1 Model

Michael E. McCormick, David R. B. Kraemer,
Patrick Hudson, and William Noble

November 2002

20030109 071
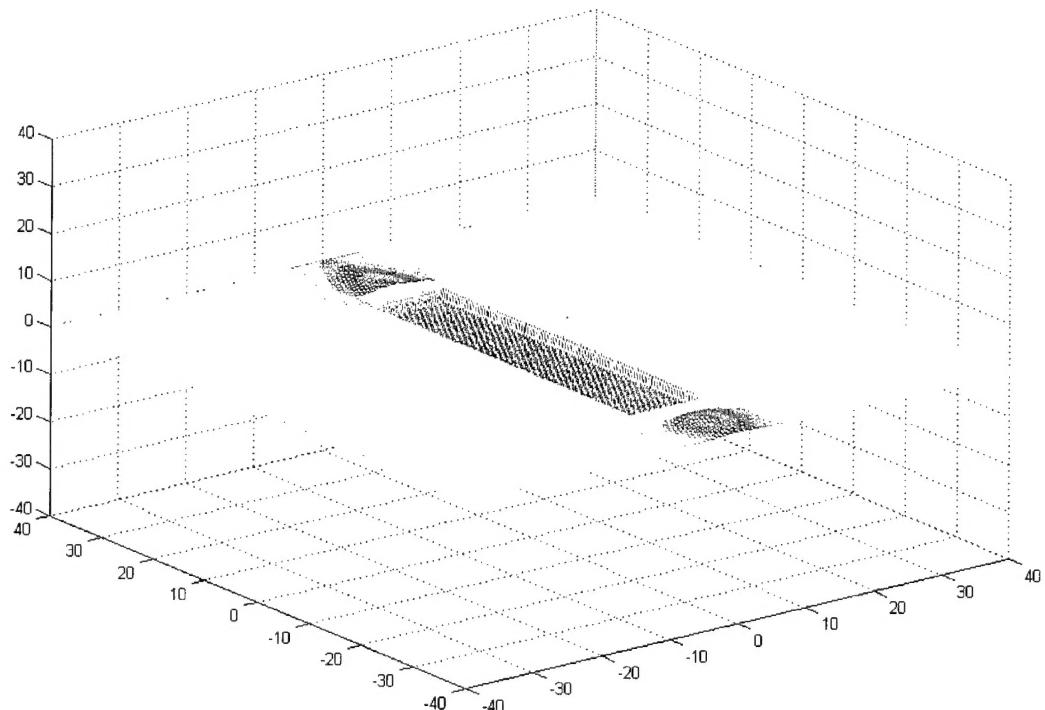
Analysis of the Added Mass of a Barge in Restricted Waters

Phase 1 Model

by   Michael E. McCormick, David R. B. Kraemer,
Patrick Hudson, William Noble

Department of Civil Engineering
The Johns Hopkins University
3400 N. Charles Street
Baltimore, MD 21218-2686

Final report

Contents

List of Figures

Preface

The work described in this report was authorized by Headquarters, U.S. Army Corps of Engineers (HQUSACE), as part of the Innovations for Navigation Projects (INP) Research Program. The work was performed under Work Unit (WU) 33143, "Design of Innovative Lock Walls for Barge Impact." The work was initiated by Mr. Robert C. Patev, former Principal Investigator of WU 33143. Current Principal Investigator is Dr. Robert M. Ebeling of the U.S. Army Engineer Research and Development (ERDC) Information Technology Laboratory (ITL).

Dr. Tony C. Liu was the INP Coordinator at the Directorate of Research and Development, HQUSACE; Research Area Manager was Mr. Barry Holliday, HQUSACE; and Program Monitors were Mr. Mike Kidby and Ms. Anjana Chudgar, HQUSACE. Mr. William H. McAnally of the ERDC Coastal and Hydraulics Laboratory was the Lead Technical Director for Navigation Systems; Dr. Stanley C. Woodson, ERDC Geotechnical and Structures Laboratory (GSL), was the INP Program Manager.

This report was prepared by Drs. Michael E. McCormick, David R. B. Kraemer, Patrick Hudson, and William Noble of The Johns Hopkins University, Department of Civil Engineering, Baltimore, MD.

This research was monitored by Dr. Ebeling, under the supervision of Mr. H. Wayne Jones, Chief, Computer-Aided Engineering Division, ITL, Dr. Jeffery P. Holland, Director, ITL; and Dr. David W. Pittman, Acting Director, GSL.

At the time of publication of this report, Dr. James R. Houston was Director of ERDC, and COL John W. Morris III, EN, was Commander and Executive Director.

1   Introduction, Analysis, and Application

Background

In a simple towing-tank experiment, the free surface excited by the forward motion of a barge model was studied. Sketches of the model and tank are shown in Figures 1-3. Several rather important observations were made during this two-dimensional (approximately, since the model spanned the channel) study of a rectangular barge in a narrow channel. First, when the towing speed was low enough, no dispersive surface waves were created. Instead, the free-surface elevation at the bow was found to increase as the model increased speed; while, at the stern, the free-surface drawdown increased with speed. This latter observation was somewhat obscured by wake effects. As the speed of the body increased, dispersive surface waves were created, producing rather interesting reactions on the model in the narrow channel. These reactions will be addressed in Phase 2 of the present study. In this report, an analytical, three-dimensional added-mass study is presented. The analytical model developed herein is based on the low-speed (0 to 4 fps (0 to 1.2 m/s)) free-surface behavior observed in the tank study.

Analysis

The mathematical model developed in this study describes a barge approaching a quay wall at angle α, as diagrammed in Figure 4. In that figure, we see an areal water-plane diagram of the approaching barge on the left-hand side and its mirror image on the right-hand side. The use of the mirror image allows for the effects of the presence of the quay wall. Two inertial coordinate systems are used, along with three linear coordinates (X_a, X_c, and s) on the physical barge and three linear coordinates (X_a', X_c', and s') on the image barge. The first inertial system (ξ, ζ, z) has ξ on the line of action of the approaching physical barge; the second system (ξ', ζ', z) has ξ' on the line of action of the barge image. The origins of the two inertial coordinate systems are at the same point on the quay wall, where the calm-water level intersects the wall. The relationships among these are

$$\xi' = \xi \cos(2\alpha) + \zeta \sin(2\alpha) \tag{1a}$$
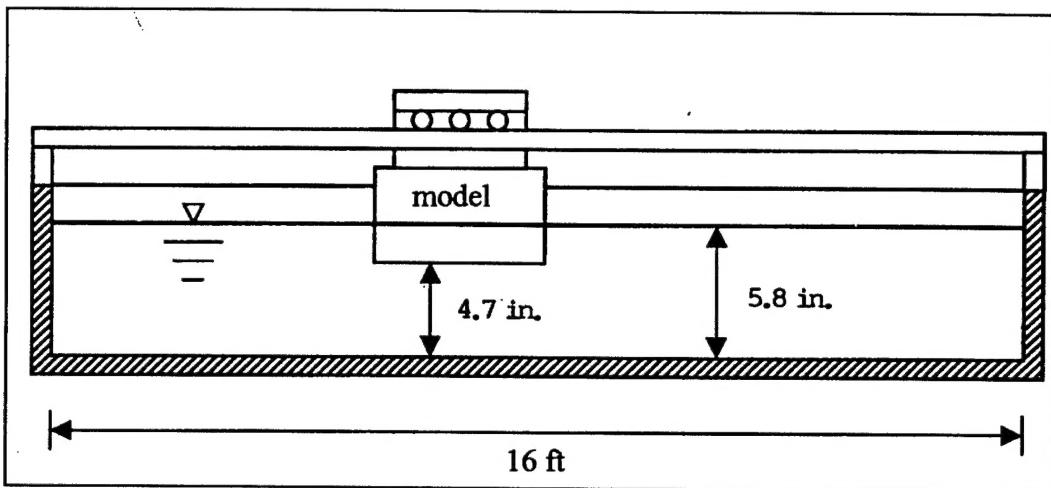
Figure 1.   Elevation view sketch of model and tank (not to scale)
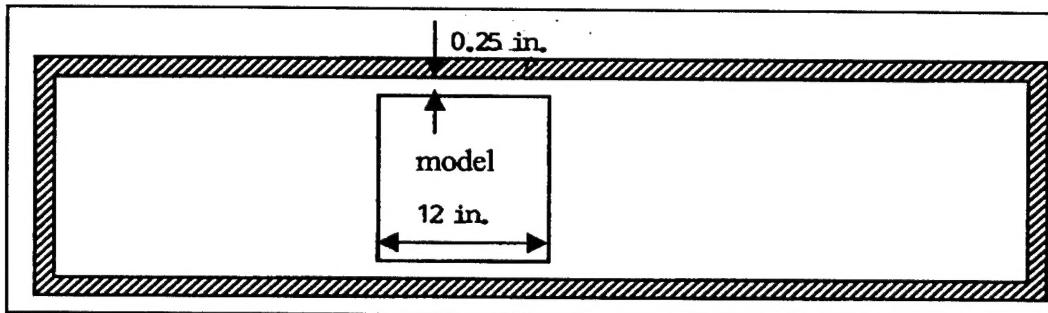
Figure 2.   Plan view sketch of model and tank (not to scale)
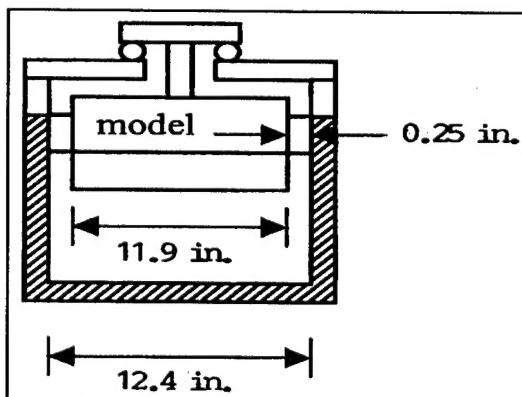
Figure 3.   Cross-sectional view sketch of
             model and tank (not to scale) (to
             convert inches to millimeters,
             multiply by 25.5)
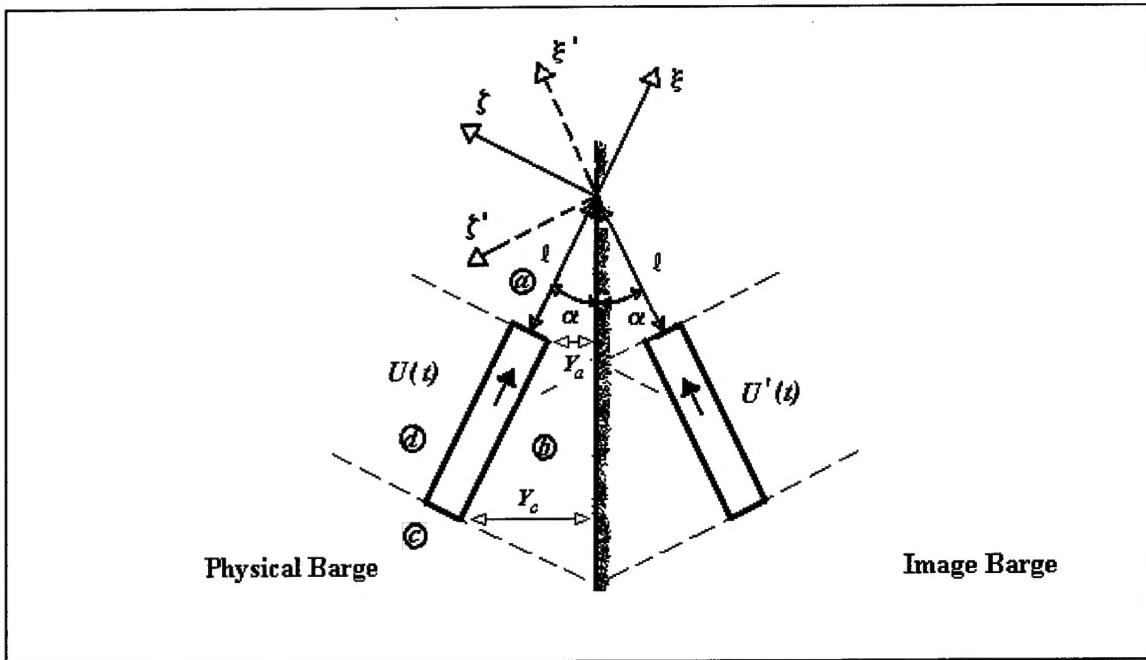
Figure 4.   Water-plane sketch of barge approaching the quay and its mirror image

$$\zeta' = -\xi \sin(2\alpha) + \zeta \cos(2\alpha) \tag{1b}$$

Referring to the sketch in Figure 5, the relationships between the physical barge coordinates are

$$s = \xi + \frac{L}{2} + \ell(t) \tag{2a}$$

$$X_a = s - \frac{L}{2} + X_0 = \xi + \ell(t) + X_0 \tag{2b}$$

$$X_c = s - \frac{L}{2} + X_0 = \xi + L + \ell(t) + X_0 \tag{2c}$$

where

L = wetted length of the barge

$\ell(t)$ = distance between the leading edge of the barge along the line of action in the center plane of the barge and the quay wall

X_0 = distance between the nodes of the free-surface deflection and intersections of the bow and stern with the calm-water plane along the center plane
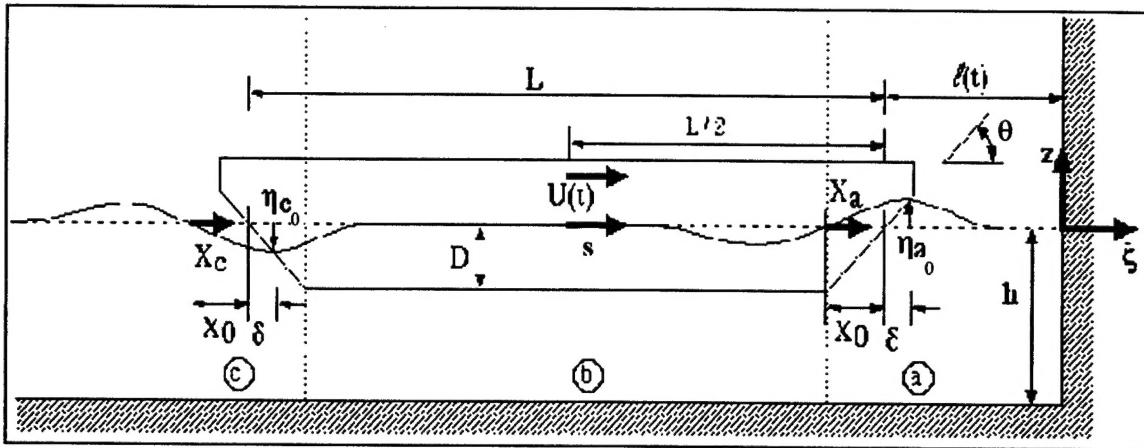
Figure 5. Elevation sketch of physical barge and free surface

Between the barge coordinates of the physical and image barges, the following relationships exist:

$$X'_{a,c} = X_{a,c}[2\cos(\alpha)-1] + \frac{W}{2}\sin(2\alpha) + 2Y_{a,c}\sin(\alpha) \tag{2d}$$

$$\zeta'_{a,c} = \zeta_{a,c}[2\cos(\alpha)-1] - X_{a,c}\sin(2\alpha) + W\cos^2(\alpha)$$
$$+ 2Y_{a,c}\cos(\alpha) \tag{2e}$$

where the double subscripts (a,c) are used for brevity. Referring to Figure 4, the distances $Y_a(t)$ and $Y_c(t)$ [$= Y_a(t) + L\sin(\alpha)$] are those between the respective bow and stern barge corners on the starboard side and the wall on the water plane. We should note, here, that in the application of the analysis, two barge orientations are of special interest. The first is when the barge is traveling parallel to the quay wall at a separation distance Y_a from the wall to the barge side. For this condition, $\alpha = 0$, and the image barge coordinates are

$$X'_{ap} = X_{ap} = X'_{cp} \tag{2f}$$

$$\zeta'_{ap} = \zeta_{ap} + W + 2Y_{a,cp} = \zeta'_{cp} \tag{2g}$$

where W is the barge wetted width and the subscript p refers to the *parallel travel*. The second orientation is when the barge is normal to the wall, and for this, the subscript n is used. The image barge coordinates for this orientation are

$$X'_{an} = -X_{an} + 2Y_a \tag{2h}$$

$$\zeta'_{an} = -\zeta_{an} = -\zeta_{cn} \tag{2i}$$

$$X'_{cn} = -X_{cn} + 2(Y_a + L) \tag{2j}$$

For the general case considered here, we can assume that the barge has a constant acceleration (or deceleration), or that the barge is running at a constant speed. Hence, the barge speed is

$$U(t) = U_0 + a_0 t \tag{3}$$

where U_0 is an initial barge speed and a_0 is a constant acceleration if positive, or a constant deceleration if negative. The origins of X_a and X_c are at the free-surface nodes of the respective bow and stern wave forms, as sketched in Figure 5.

Hydrodynamics about the physical barge

The analysis is first applied to the physical barge (as opposed to the image barge). Our attention is focused on the free surface in the neighborhoods of the bow and the stern. From experimental observations, the free surface is assumed to have bow and stern profiles, as sketched in Figure 5. Ahead of the bow, there is a crest at $s = L/2 + \delta$ and a node at $s = L/2 - X_0$. At the stern, a trough is at $s = -L/2 + \delta$, and the node is at $s = -L/2 - X_0$. The distance δ is to be determined by rake angles at the bow and the stern. In both $-X_0 \leq X_a \leq X_0$ and $-X_0 \leq X_c \leq X_0$, the free surface is assumed to have the properties of a ship-generated, deep-water, linear wave.

From McCormick (1973), the "half-wavelength" in these regions is

$$2X_0 = \frac{\pi}{g} U^2 \tag{4}$$

To satisfy the assumed free-surface profile, the following potential function is assumed:

$$\varphi_{PB} = \varphi_{bow} + \varphi_{stern} \tag{5}$$

$$\varphi_{PB} = -\Phi(t)\left[\frac{1}{\cosh(AX_a)} \frac{1}{\cosh(B\zeta)} - \frac{1}{\cosh(AX_c)} \frac{1}{\cosh(B\zeta)} \right] \frac{\cosh[C(z+h)]}{\cosh(Ch)}$$

where the coordinate is fixed to the barge and the subscript PB refers to the *physical barge*. The ζ-term results from the assumption that there is a negligible beam-wise velocity component over the beam of the barge traveling slowly. That velocity component has nonzero values beyond the barge sides. The wave form is traveling with respect to the inertial coordinate system, since $\ell + X_0$ in Equations 2 and 3 is a function of time. The coefficient $\Phi(t)$ varies in time due to the time-dependent velocity of the barge. Because the velocity is assumed to be small, the coefficient is a weak function of t. By this, we mean that the time derivatives of the coefficient are of second order. The first terms in the brackets

of Equation 5 represent the bow wave-form potential, while the second terms represent that of the stern.

We assume that the heights of the bow and stern wave forms are equal. Note that when viscosity is considered, the stern wave form is reduced in height due to the vortices being shed from the bottom. This is discussed later in the report.

To obtain the shape of the free surface associated with the velocity potential, we apply the linearized Bernoulli's equation at the free surface. The resulting expression for the free-surface displacement is

$$
\eta_{PB} = -\frac{1}{g}\frac{\partial \varphi}{\partial t}\bigg|_{z=0} = \frac{A\Phi U}{g}
\begin{bmatrix}
\dfrac{\dfrac{\tanh(AX_a)}{\cosh(AX_a)}\dfrac{1}{\cosh(B\zeta)} - \dfrac{\tanh(AX_c)}{\cosh(AX_c)}}{\dfrac{1}{\cosh(B\zeta)}}
\end{bmatrix}
\tag{6}
$$

Figures 6 and 7 show plots of the free-surface displacement described by Equation 6. In the region of the barge, the free surface is replaced in the plot by the boundary surface of the barge. The free-surface form approximately predicted by expression in Equation 6 is supported by experimental observations. Note that for a time-dependent speed, the separation length between the origin of X_a and the wall can be represented by

$$
(\ell + X_0) = -\int U dt
\tag{7}
$$

Hence, we can also write $d(\ell + X_0)/dt = -U(t)$. The approximation in Equation 6 is, again, based on the assumption that the barge moves slowly enough to cause the coefficients Φ, A, and B to be weak functions of time. By this we mean that the time derivatives of these functions are of second order.

In the vertical direction, the behavior of the velocity potential of Equation 5 must be like a linear wave. This behavior satisfies the bottom boundary condition, which requires that there be no normal flow at $z = -h$. The parameter C is the wave number for this linear wave. The wavelength, λ, is estimated from Equation 4, so that

$$
C = \frac{2\pi}{\lambda} = \frac{2\pi}{4X_0} = \frac{g}{U^2}
\tag{8}
$$

At the wave crest at the bow and trough at the stern ($X_a = X_0 + \delta$ and $X_c = X_0 + \delta$, respectively), we require that the slope of the free surface be equal to zero. Applying this condition along the center plane of the barge, where $\zeta = 0$, one finds that
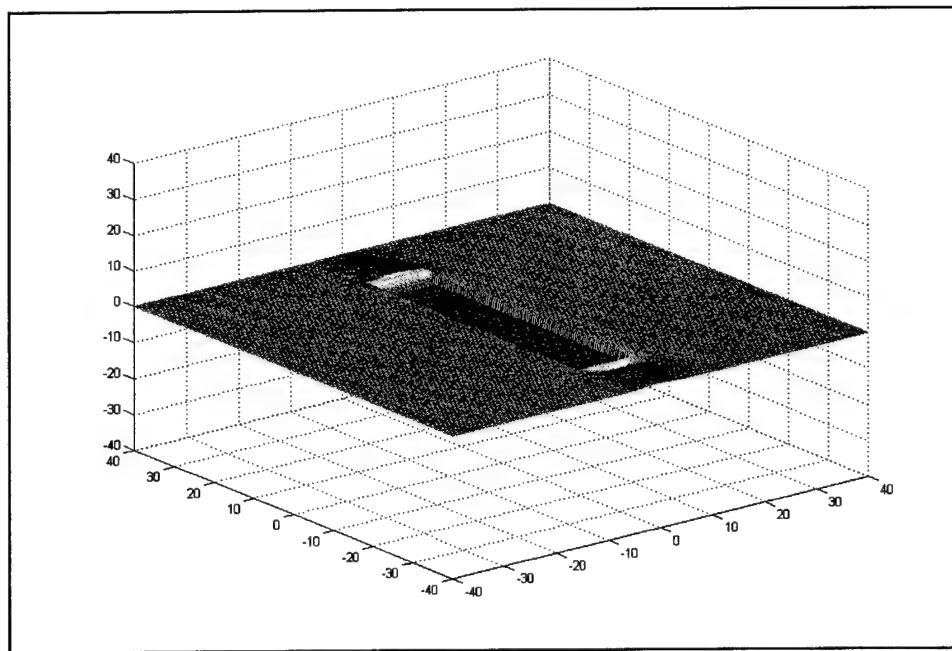
Figure 6.   Free surface surrounding jumbo open-hopper barge (JOHB) at a
speed of 10 fps
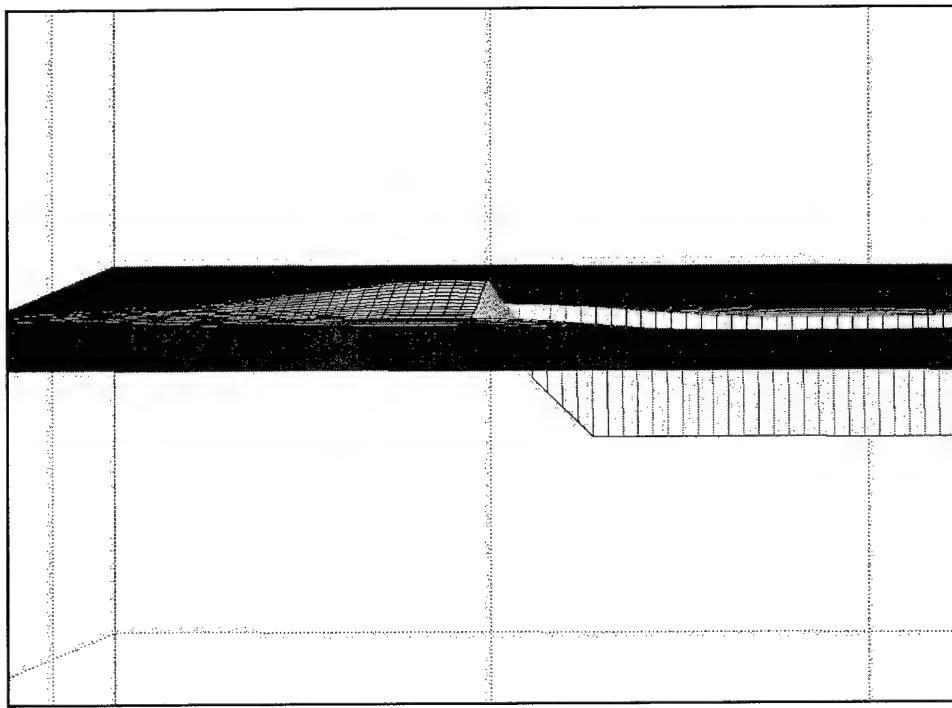
Figure 7.   Free surface surrounding bow of JOHB at a speed of 10 fps

$$\frac{\partial \eta_{PB_a}}{\partial \xi}\bigg|_{X_a=X_0+\delta,\,\zeta=0} = \frac{A^2\Phi U}{g}\left[\frac{-1}{\cosh^3(AX_a)} + \frac{\tanh^2(AX_a)}{\cosh(AX_a)}\right] = 0 \qquad (9)$$

The nontrivial solution of Equation 9 is

$$\sinh^2[A(X_0+\delta)] - 1 = 0 \qquad (10)$$

Using Equation 4 to substitute for X_0, substituting for δ using the geometry of Figure 5, and solving for the parameter A yields

$$A = \frac{1.7627g}{U^2\left(\pi + \dfrac{1}{\tan\theta}\right)} \qquad (11)$$

The velocity potentials at the bow and stern should satisfy the equation of continuity in the form of Laplace's equation

$$\nabla^2\varphi = 0 \qquad (12)$$

Applying Laplace's equation to the velocity potential of Equation 5 yields

$$\nabla^2\varphi_{PB} = -\Phi(t)\frac{\cosh[C(z+h)]}{\cosh(Ch)}\left\{A^2\left[\frac{-1}{\cosh^3(AX_a)} + \frac{\tanh^2(AX_a)}{\cosh(AX_a)}\right]\frac{1}{\cosh(B\zeta)}\right.$$

$$+ B^2\frac{1}{\cosh(AX_a)}\left[\frac{-1}{\cosh^3(B\zeta)} + \frac{\tanh^2(B\zeta)}{\cosh(B\zeta)}\right] \qquad (13)$$

$$\left. + C^2\frac{1}{\cosh(AX_a)}\frac{1}{\cosh(B\zeta)}\right\} = 0$$

On the center line of the barge in the region of the bow, Equation 13 simplifies to

$$\nabla^2\varphi_{PB_a}\bigg|_{\zeta=0} = A^2\left[\frac{-1}{\cosh^3(AX_a)} + \frac{\tanh^2(AX_a)}{\cosh(AX_a)}\right]$$

$$- \frac{B^2}{\cosh(AX_a)} + \frac{C^2}{\cosh(AX_a)} = 0 \qquad (14)$$

Letting X_a go to zero at the bow yields

$$-A^2 - B^2 + C^2 = 0 \qquad (15)$$

Solving for B,

$$B = \sqrt{C^2 - A^2} \tag{16}$$

Next, we know that points of the maximum and minimum free-surface displacements from the calm-water plane at the barge's center plane ($\zeta = 0$) are the points of the water's maximum energy absorption from the barge. The potential energy per unit volume of the water at these points, which is proportional to the free-surface displacement at these points (η_{a0} and η_{c0} in Figure 5), is equal to the water's kinetic energy per unit volume at the bow. Hence, by incorporating the expression in Equation 6, we can write the following expression for the maximum free-surface displacements:

$$\eta_{a_0} = -\eta_{c_0} = \frac{A\Phi U}{g}\left\{\frac{\tanh[A(X_0 + \delta)]}{\cosh[A(X_0 + \delta)]}\right\} \approx \frac{1}{2g}U^2 \tag{17}$$

where Φ is to be determined. Recall that $X_0 = \pi U^2/2g$ from Equation 4. Also, from the geometry shown in Figure 5, $\delta = \eta_{a0}/\tan(\theta)$. The result in Equation 17 can be rearranged to obtain the following expression:

$$\Phi = \frac{U}{2A}\frac{\cosh^2\left[\frac{AU^2}{2g}\left(\pi + \frac{1}{\tan\theta}\right)\right]}{\sinh\left[\frac{AU^2}{2g}\left(\pi + \frac{1}{\tan\theta}\right)\right]} \tag{18}$$

where θ is the rake angle.

In summary, the respective coefficients A, B, C, and Φ of Equations 11, 16, 8, and 18 are parametric. The parameters are time dependent if the motion of the barge is unsteady, i.e., if $U = U(t)$.

In the following section, the velocity potential and free surface of the image barge is presented. This is, again, done in the barge coordinate system. Hence, we use the coordinate relationships in Equations 2d and 2e in expressions of the forms of Equations 5 and 6.

Free surface about the mirror-image barge

The velocity potential and free-surface displacement expressions for the mirror-image barge are similar to those in Equations 5 and 6, respectively. The differences are in the coordinates, as expressed in Equation 1. In terms of the physical barge coordinates, the velocity potential for the mirror image is

$$\varphi_{IB} = -\Phi(t) \left[\frac{1}{\cosh(AX'_a)} \frac{1}{\cosh(B\zeta')} - \frac{1}{\cosh(AX'_c)} \frac{1}{\cosh(B\zeta')} \right] \frac{\cosh[C(z+h)]}{\cosh(Ch)} \quad (19)$$

and the free-surface displacement is

$$\eta_{IB} = \frac{A\Phi U}{g} \left[\frac{\tanh(AX'_a)}{\cosh(AX'_a)} \frac{1}{\cosh(B\zeta')} - \frac{\tanh(AX'_c)}{\cosh(AX'_c)} \frac{1}{\cosh(B\zeta')} \right] \quad (20)$$

where $X'_{a,c}$ and $\zeta'_{a,c}$ are obtained from Equations 2d and 2e, respectively.

The results in Equations 5 and 20 can be added together to obtain the expression for the velocity potential at any point in the physical flow field ($\xi \leq 0$ in Figure 4). That is, for any point in the physical flow field, the velocity can be obtained from the following velocity potential:

$$\varphi = \varphi_{PB} + \varphi_{IB} \quad (21)$$

In addition, the free-surface displacement expressions of Equations 6 and 21 are added together to obtain the free-surface geometry in the physical field. The result is that

$$\eta = \eta_{PB} + \eta_{IB} \quad (22)$$

We shall use these expressions to obtain the added mass excited by the physical barge.

Kinetic energy and added mass

As derived by Karamcheti (1966) and other books dealing with advanced fluid mechanics, the kinetic energy of a potential flow that is caused by a body traveling at a speed U is mathematically expressed as

$$T = -\frac{\rho}{2} \iint_S \varphi \frac{\partial \varphi}{\partial n} dS = -\frac{\rho}{2} \iint_S \varphi \nabla \varphi \cdot dS = -\frac{1}{2} m_w U^2 \quad (23)$$

where (referring to the sketches in Figures 8-10),

ρ = mass density of the ambient water

n = normal unit surface vector at any place on the surface area (S) of the barge

m_w = added mass
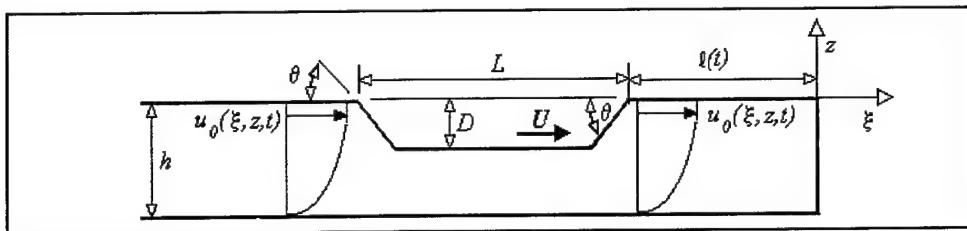
Figure 8. Relative and absolute flow directions in the center plane
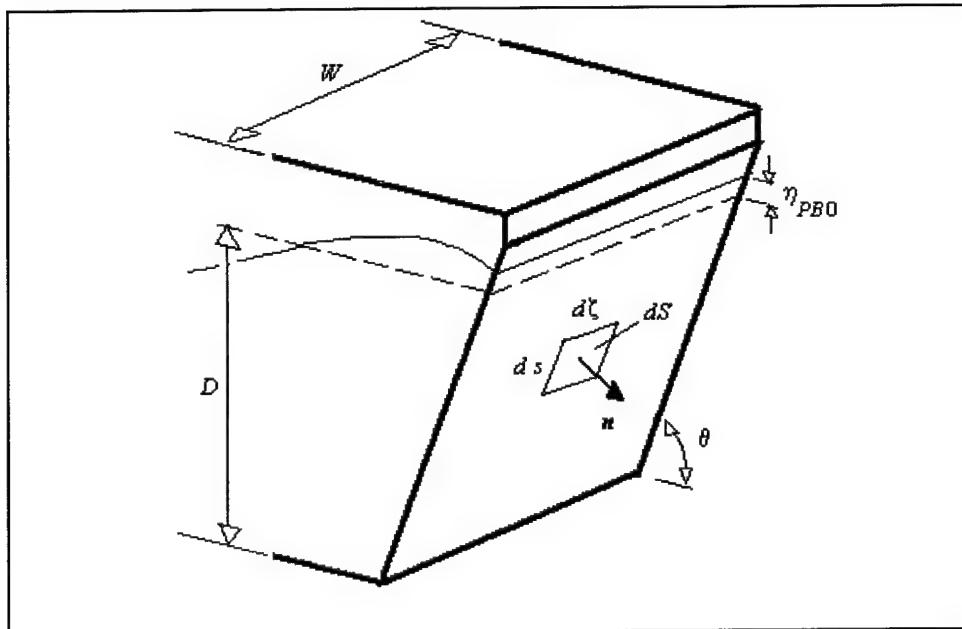
Figure 9. Nomenclature for the bow and stern of the physical barge
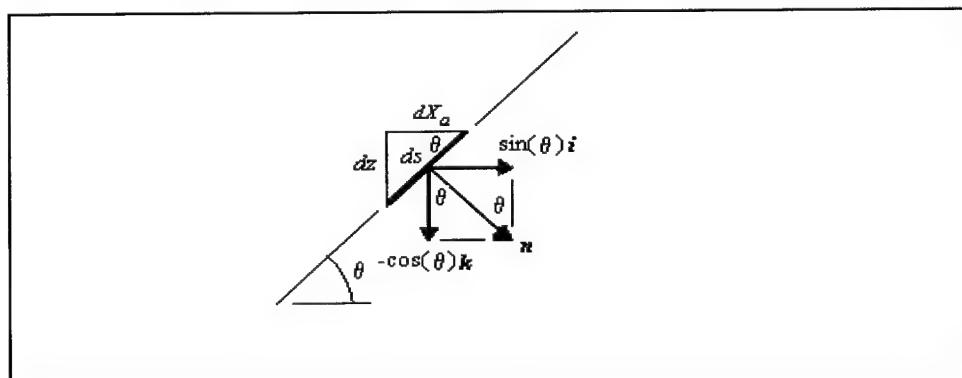
Figure 10. Norman (surface) unit vector relationships

The added mass is a measure of the inertial reaction of the fluid on the barge. From Equation 23, then, the added-mass expression is

$$m_w = \frac{\rho}{U^2} \iint_S \varphi \frac{\partial \varphi}{\partial n} dS = \frac{\rho}{U^2} \iint_S \varphi \nabla \varphi \cdot dS \tag{24}$$

Equation 24 is solved numerically. The results are applied to a jumbo open-hopper barge for various values of the parameters and approach angle. Appendix A presents the computer program used to obtain the results described herein. Example input and output runs are shown in Appendix B.

Application to the Surfaces of the Physical Barge

To determine the added mass, one applies Equation 24 to each surface of the body using each of the velocity potentials. On the bow surface,

$$\left.\frac{\partial \varphi}{\partial n}\right|_{bow} = \frac{\partial \varphi}{\partial \xi} \sin\theta - \frac{\partial \varphi}{\partial z} \cos\theta \tag{25}$$

while on the stern,

$$\left.\frac{\partial \varphi}{\partial n}\right|_{stern} = -\frac{\partial \varphi}{\partial \xi} \sin\theta - \frac{\partial \varphi}{\partial z} \cos\theta \tag{26}$$

as seen in Figure 10.

2 Results

Before describing the results, a brief discussion should be given regarding the nature of the added mass. As previously mentioned, the added mass is a measure of the inertial reaction of a fluid on the motion of a body. When the body is at rest, the added mass is, naturally, equal to zero. When a body travels at a constant velocity, there is a convective acceleration of the fluid. Hence, even at a constant body speed, there is an inertial reaction from the fluid, as exhibited by the added mass. When the body accelerates, the total inertial reaction equals the virtual mass, which is the body mass plus the added mass. The force on the body, then, is the product of the virtual mass and the body's acceleration.

Now, concerning the results of this study, Equation 24 is applied to the jumbo open-hopper barge (JOHB), for the most part. A comparison of one of the parametric conditions for the JOHB is made with the standard open-hopper barge (SOHB). Since the geometries of the two barges are similar, the behaviors with the parameters are also similar. For the two barges, the values listed in Table 1 apply.

Table 1 Comparison of Parametric Conditions, Jumbo and Standard Open-Hopper Barges		
Parameter	JOHB	SOHB
Wetted length (L), ft [m]	195 [59]	175 [53]
Wetted beam (W), ft [m]	35 [11]	26 [8]
Draft (D), loaded,[1] ft [m]	10[1] [3]	10[1] [3]
Draft (D), unloaded, ft [m]	3 [0.9]	3 [0.9]
Displacement, loaded, short tons [million kg]	1,500 [1.4]	1,000 [0.9]
Displacement, unloaded, short tons [million kg]	279 [0.25]	179 [0.16]
Rake angle, θ (for computations)	Variable	Variable
[1] The loaded draft is used as the standard.		

Effect of Barge Speed in Open Waters

Since the barge speed is assumed to have low values in confined waterways, the maximum speed value used herein is 4 fps (1.2 m/s). The "added weight"

(m_wg) is presented in Figure 11 as a function of barge speed for the JOHB traveling in open waters, where the operating water depth (h) is 18 ft (5.5 m). The JOHB parametric values are listed in Table 1; a rake angle of 45 deg was used for the JOHB in all computations. The added weight is chosen so that a direct comparison can be made with the displacement tonnage of the barge. The "jump" in the plot could result from the passage of the barge through the critical speed in the wave-resistance curve (see, for example, McCormick 1973). Further investigation of this is warranted in Phase 2 of this research.

Effect of Water Depth in Open Waters

In Figure 12, the added weight is shown as a function of water depth at a position well away from the wall. Again, the parameters used are those of the JOHB in Table 1 (rake angle, 45 deg).

Effect of Barge-Wall Separation and Barge Load

Because of the rake angle of the bow (45 deg), the only separation effect occurs when the barge travels parallel to the quay wall. The wall effect extends only several feet from the wall, as can be seen in the results presented in Figure 13. Hence, for all but the smallest of approach angles (α), there is no wall effect, according to the theory. This is due to the low barge speed. The results are presented for the JOHB under both loaded and unloaded conditions.

Rake Angle Effect

Although the rake angles of both the JOHB and the SOHB are fixed, the effect of rake angle is presented in Figure 14. As can be seen in that figure, there appears to be an angle for which the added weight is maximum. The purpose of this exercise is to help barge designers determine an optimum configuration.

Comparison of the JOHB and SOHB

In this case, the JOHB and SOHB are compared under loaded conditions, operating in 18 ft (5.5 m) of water, at a speed of 3 fps (0.9 m/s). For the JOHB, the added weight is 3.44 tons (3,120 kg) and, for the SOHB, 2.56 tons (2,322 kg). Although the scale factors for the two barges differ for both length and width, the behaviors in Figures 11-14 can be expected to be the same for the SOHB.
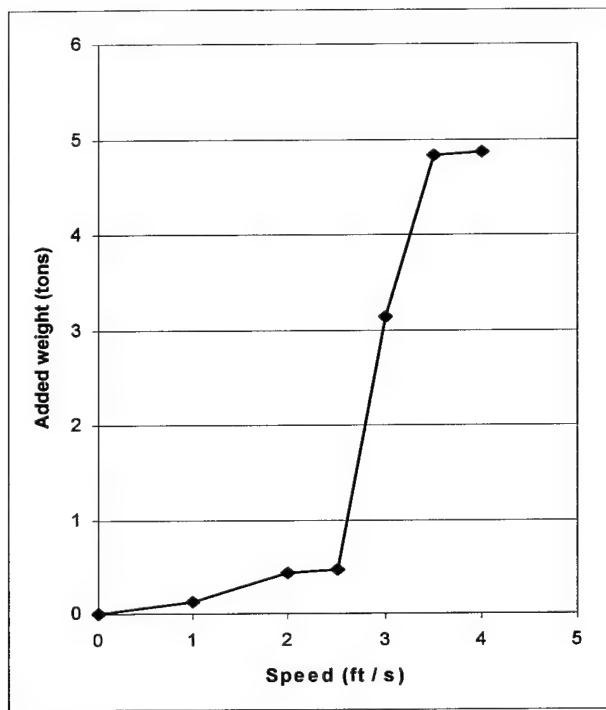
Figure 11. Added-weight variation with speed of the loaded JOHB traveling parallel to the wall in 18-ft-deep open waters
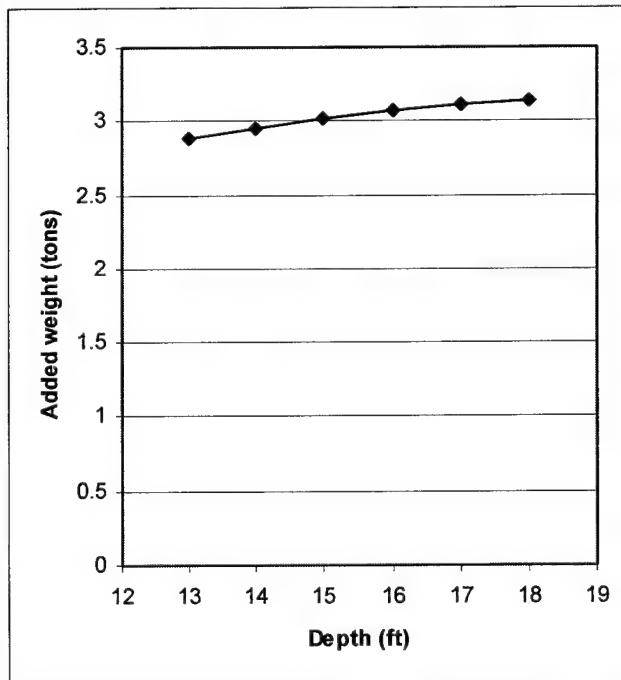
Figure 12. Water depth effect on the added weight of the loaded JOHB traveling parallel to the quay wall at a speed of 3 fps
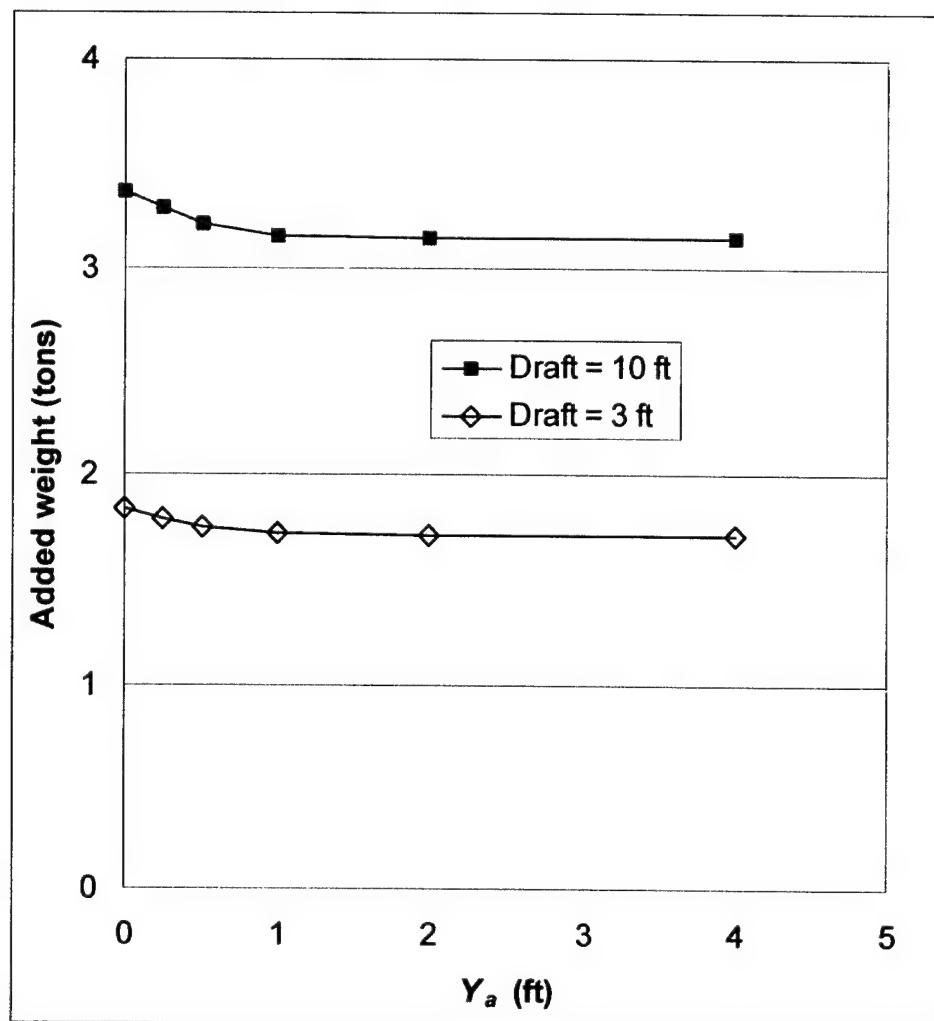
Figure 13. Wall effects on the added weight of the loaded and unloaded JOHB traveling parallel to the quay wall in 18 ft of water at a speed of 3 fps. Here, Y_a is the distance between the starboard corner of the barge and the wall, measured perpendicular to the wall)
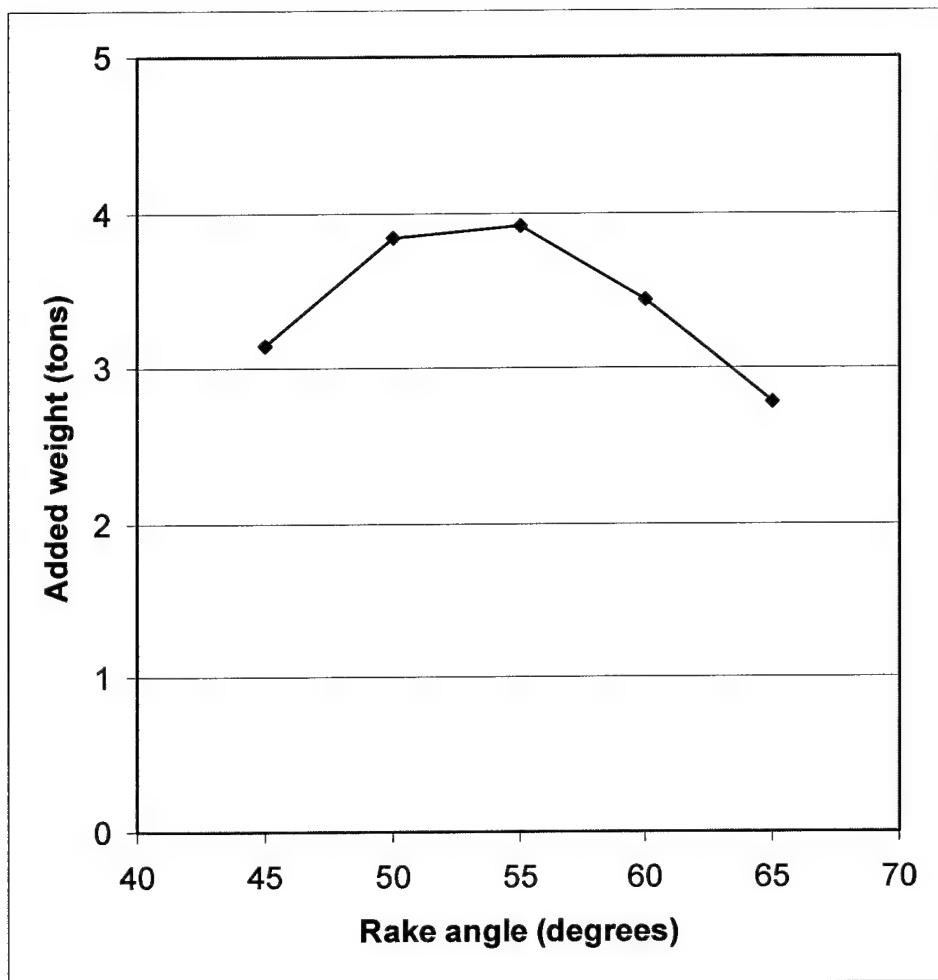
Figure 14.   Effect of rake angle of the JOHB operating in 18-ft-deep open
             waters at a speed of 3 fps

3 Discussion and Conclusions

The objective of this study is to mathematically model the added mass of a barge tow operating in restricted waters, i.e., waters of finite depth that are bounded by a vertical wall. The model is based on the free surface altered by a box-lighter (a barge with vertical sides, bow, and stern) towed in the wave/ towing tank at the Johns Hopkins University.

The barge model was towed using a gravity towing system. Hence, the acceleration in the ideal case is constant. The realities of viscosity and the presence of a vertical channel wall placed in front of the towed model, however, produced a varying resisting force and therefore a varying acceleration over the test runs. One cause of the varying acceleration was the changing added mass, as is discussed later.

The free-surface deflections resulting from the accelerating barge can be seen in Figures 15-17, where the respective accelerations vary from the highest to the lowest value. Because both the bow and stern of the model were vertical, the crest of the bow wave and the trough of the stern wave (due to drawdown) were at their respective barge faces. The drawdown is most apparent in Figure 17. The flow separation at the transom of the model absorbed much of the energy trans-mitted to the water. This resulted in a shallower trough than would be observed under ideal (inviscid) conditions. The free-surface profile at and near the bow could be seen in the water between the barge and the tank wall. The clearance between the two structures was approximately 0.2 in. (5 mm). The side "channels" were regions of relatively high viscous losses.

The predicted effect of the barge speed on added weight can be seen in Figure 11 for the JOHB operating in open waters where the water depth is 18 ft (5.5 m). For an unexplained reason, the added weight experiences a "jump" in values between 2 and 3 fps (0.6 and 0.9 m/s). For speeds higher than 4 fps (1.2 m/s), the values of the added weight drop as the speed increases. This is attributed to fact that the theory is a low-speed theory.

The effects of water depth on the added weight are shown in Figure 12 for the JOHB traveling at 3 fps (0.9 m/s) in 18-ft (5.5-m)-deep open waters. For the depths studied, the increase in added weight with increasing depth is nearly rectilinear.
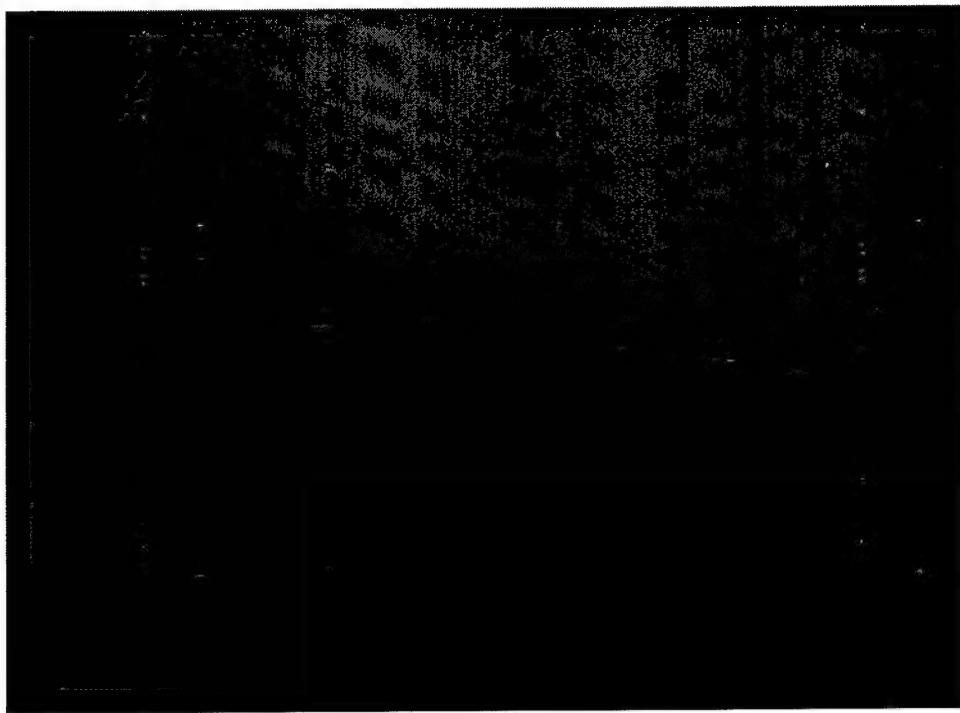
Figure 15. Free-surface profile amidship for a rectangular model—high acceleration
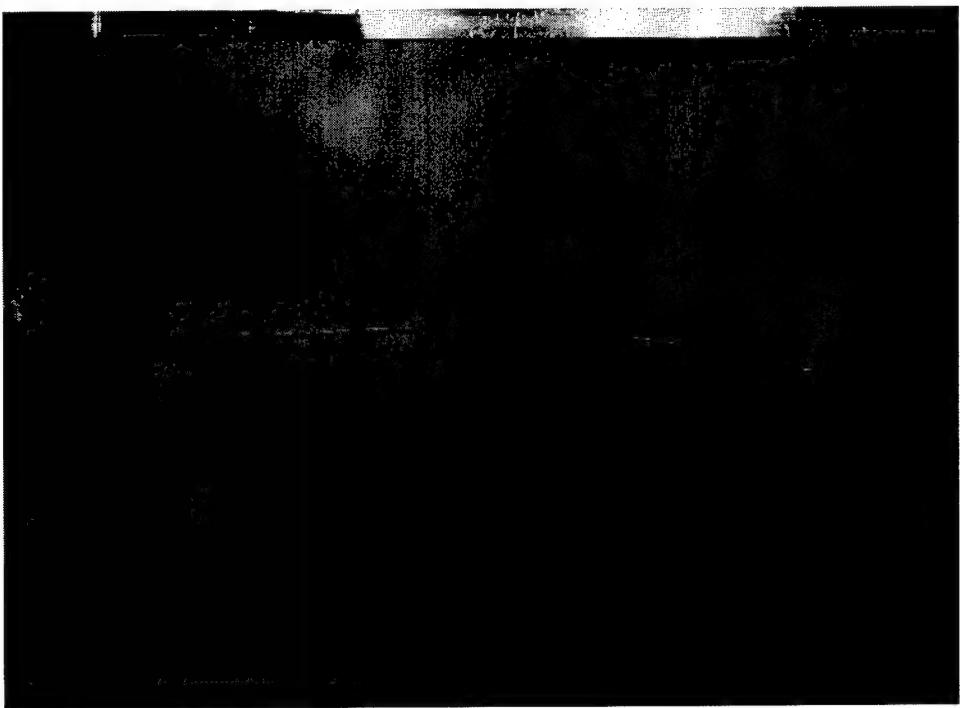

Figure 16. Free-surface bow to stern for a rectangular model—moderately high acceleration
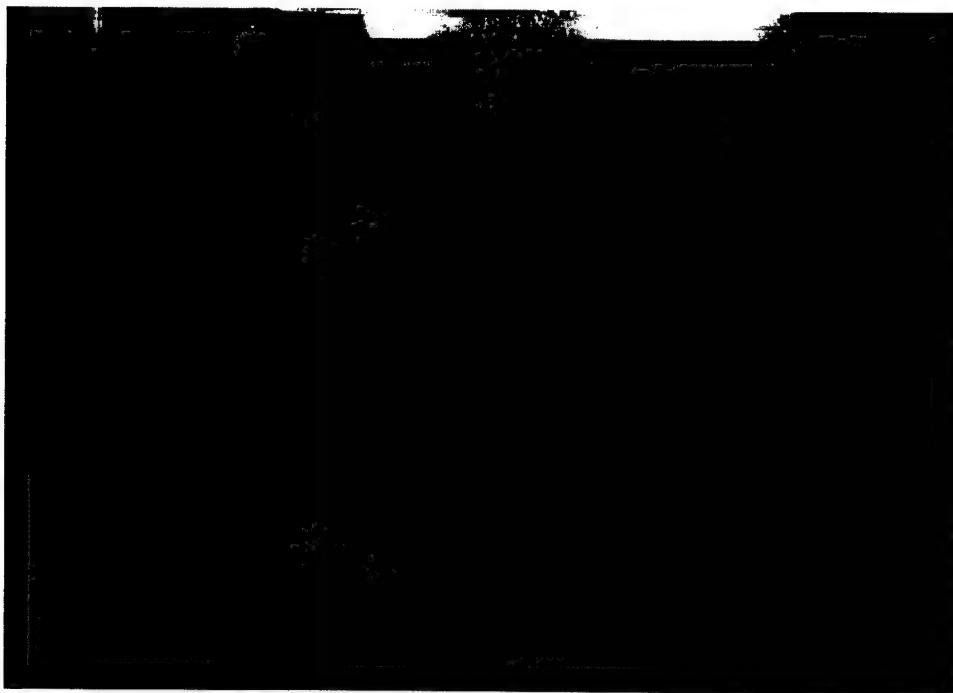
Figure 17. Free-surface profile—moderate acceleration

In Figure 13, the effect of the separation distance (Y_a) between the quay wall and the JOHB traveling parallel to the wall is shown. It can be seen in that figure that the wall effect at a 3-fps (0.9 m/s) barge speed is observed only within several feet from the wall, for both loaded and unloaded conditions.

The effect of varying the rake angle (θ) of the bow and stern of the JOHB is seen in Figure 14. In that figure, we observe a peak value of the added weight, occurring between angles of 50 and 55 deg. Depending on the added-weight effect on performance, this curve can be used to somewhat optimize the system by selecting a θ-value that is both practical and corresponds to the lowest inertial resistance.

Figure 18 shows a plot of the velocity potential contours in the water surrounding the JOHB at a velocity of 3 fps (0.9 m/s), as predicted by Equation 5. A detail of the flow around the bow of the barge is shown.

Finally, during the experiments on the model barge motions in the wave/towing tank, the barge acceleration was measured. The acceleration was integrated twice to obtain the velocity and the displacement of the model. In these tests, a vertical barrier was alternately placed in the path of the model to simulate the presence of a wall. The results of these tests are presented in Figures 19-22. Although a number of towing weights were used, only two are represented in those figures. For the low towing weight (lower acceleration runs), the presence of the wall had little effect on the speed and acceleration, as can be seen in Figure 19, where $\ell(t)$ is finite (as defined in Figures 5 and 8), and in Figure 20, where $\ell(t)$ is infinite. For the high towing weight (higher
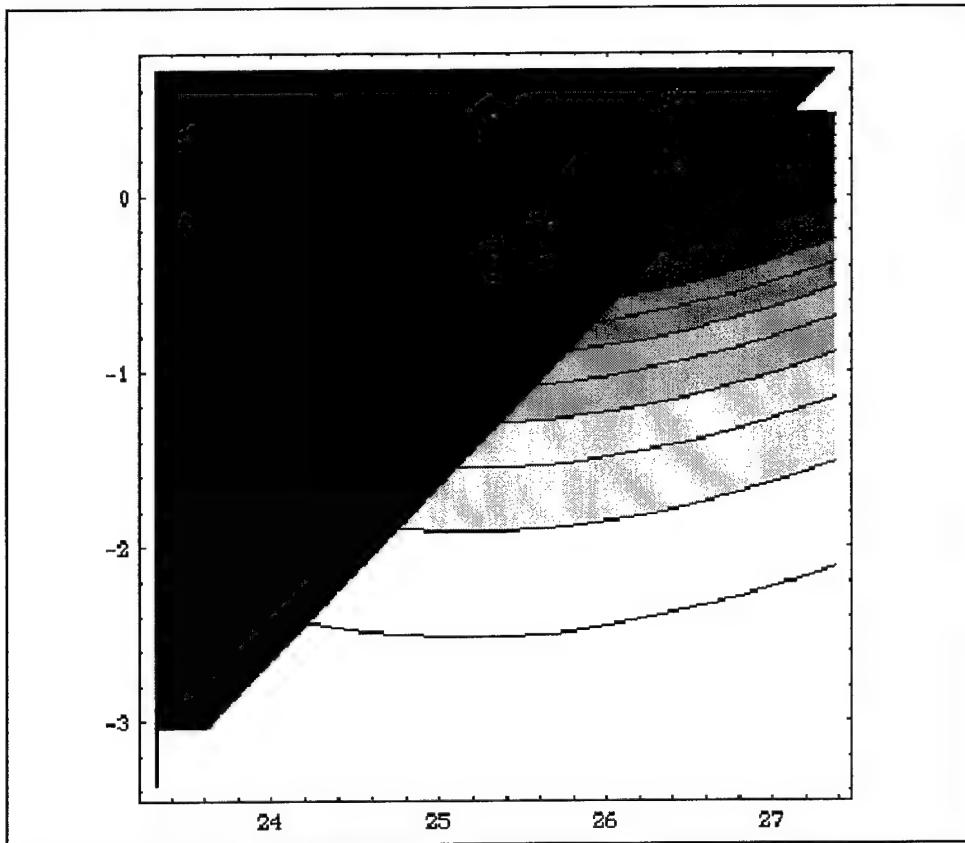
Figure 18. Velocity potential contours for JOHB at a speed of 3 fps

acceleration runs), there is a pronounced decrease in the acceleration and the corresponding velocity. Since the acceleration is a measure of the inertial reaction of the water on the model, we can conclude that the wall causes an increase in the added mass for the higher accelerations. This effect is also partially produced by the buildup in the water between the bow and wall at the higher accelerations.

For accelerations resulting in speeds that are not "low," another phenomenon is observed. That is, a traveling wave is produced by the initial bow motion that travels to the wall, reflects, and returns to the model, bringing the model to a virtual halt. This effect is actually beneficial for barge tows that are traveling at higher speeds toward vertical barriers, since it helps to prevent full-speed collisions with the wall.

This preliminary analysis has several limitations, and further study is recommended. The form of the velocity potential of Equation 5 is based on experimental observations. Although Figures 6 and 7 indicate that this potential function is a reasonable prediction, the governing equation for potential flow (Laplace's equation) is met only at specific points in the fluid domain. Furthermore, the boundary conditions for this boundary-value problem are met only at specific points, not the whole boundary surface of the barge. A
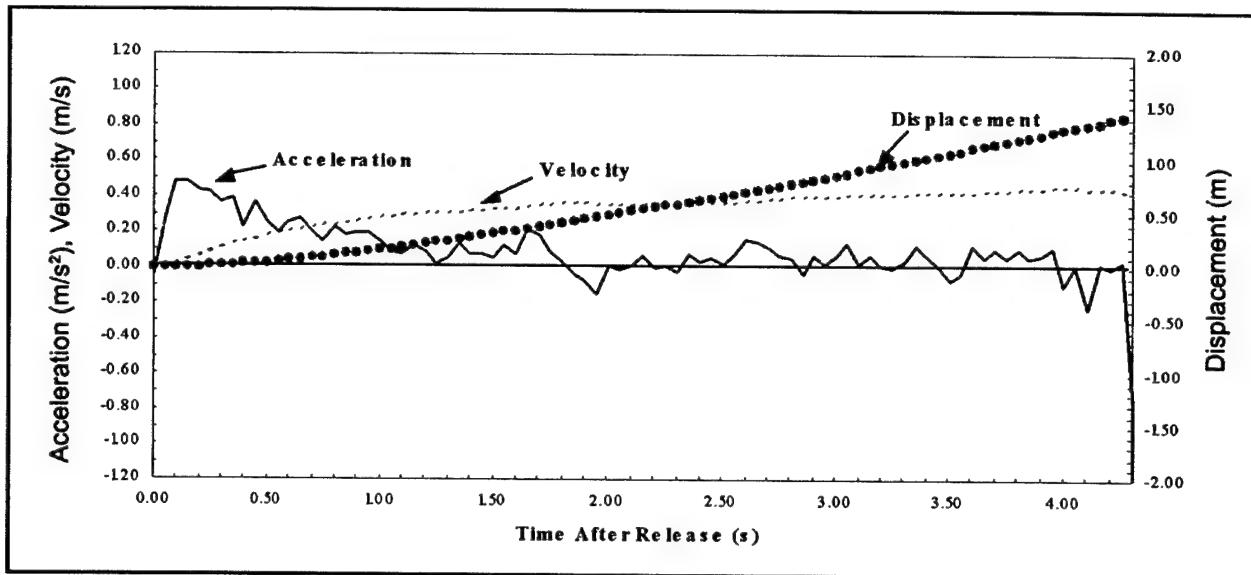
Figure 19. Model displacement, velocity, and acceleration under lower force without the wall in place
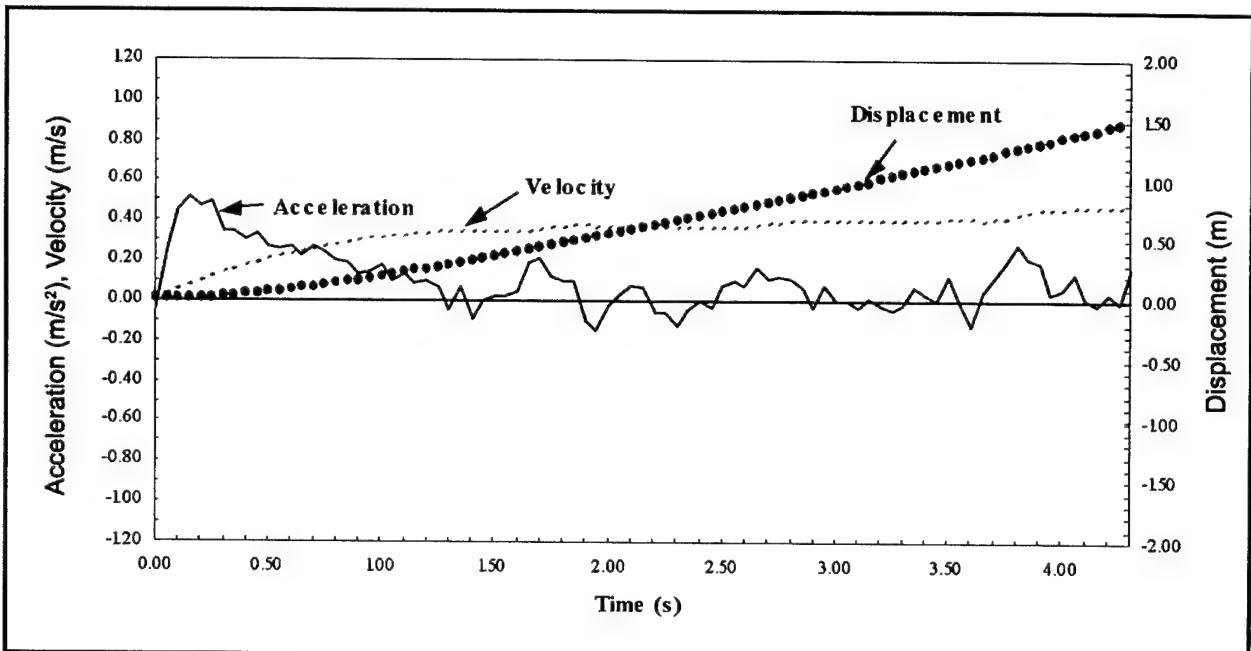


Figure 20. Model displacement, velocity, and acceleration under lower force with the wall in place
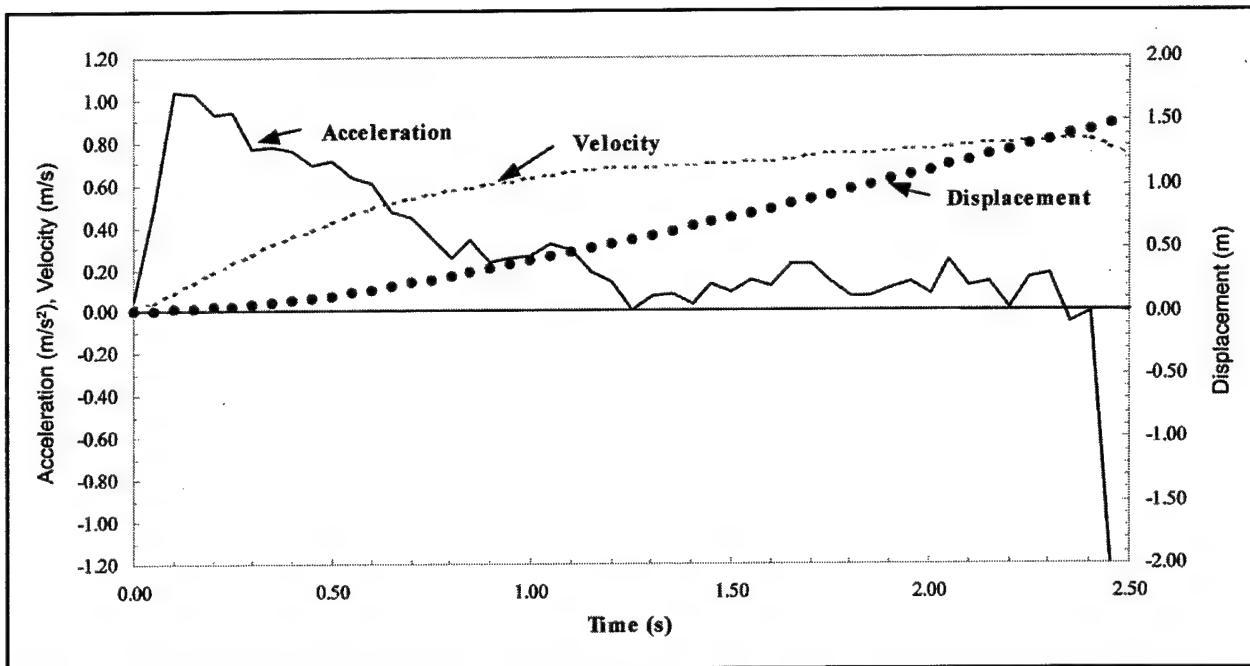
Figure 21. Model displacement, velocity, and acceleration under higher force without the wall in place
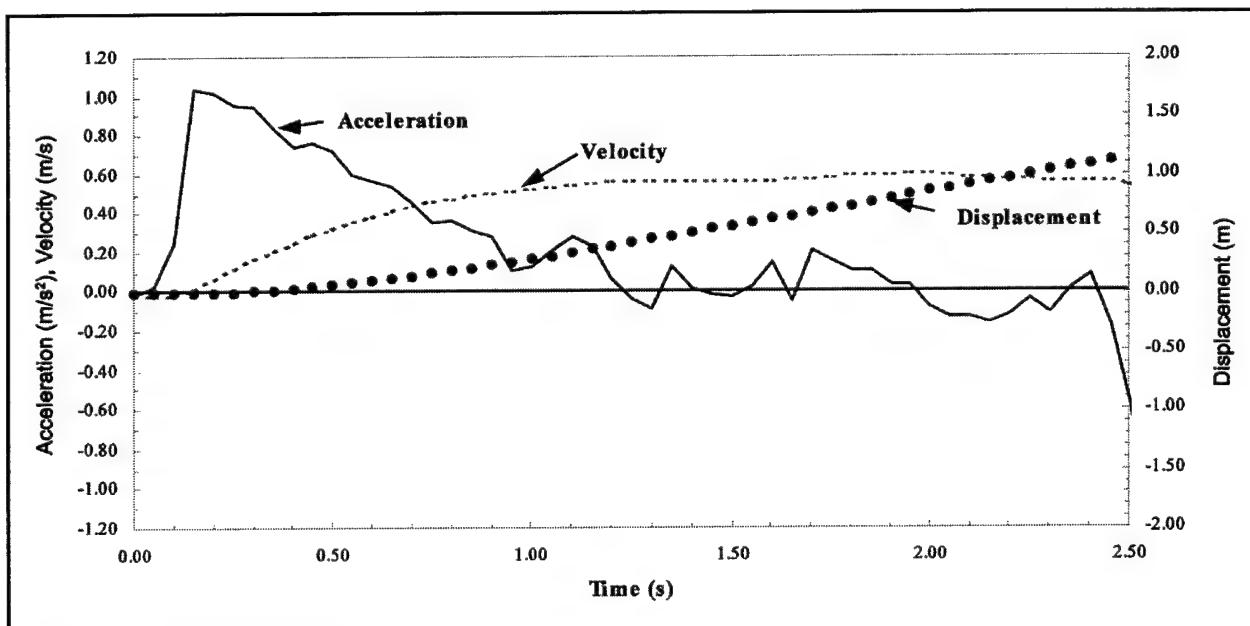
Figure 22. Model displacement, velocity, and acceleration under higher force with the wall in place

boundary-element method analysis of the problem is planned, and will solve the complete boundary-value problem.

In conclusion, the analysis presented herein is primarily heuristic, being based on experimental observations. The assumptions made limit the analysis, particularly in predicting the values of the added mass or added weight; however, it is believed that the analysis does predict the behavior of the added mass with varying parameters. A follow-on study will improve the quantitative predictions, since that study will incorporate the boundary-element method, which requires few of the assumptions made herein.

Finally, the analysis presented herein is considered to be superior to the potential theories that were based on two-dimensional models, as in the report by Wendel (1956) and the report by Brennen (1982).

References

Brennen, C. E. (1982). "A review of added mass and fluid inertial forces," Report N62583-81-MR-554, Naval Civil Engineering Laboratory, Port Hueneme, CA.

Karamcheti, Krishnamurty. (1966). *Principles of ideal-fluid aerodynamics*. John Wiley and Sons, New York.

McCormick, Michael E. (1973). *Ocean engineering wave mechanics*. Wiley-Interscience, New York.

Wendel, Kurt. (1956). "Hydrodynamic masses and hydrodynamic moments of inertia," David Taylor Model Basin Translation 260, Naval Surface Warfare Center, Carderock Division, MD.

Appendix A
FORTRAN Computer Code

This appendix presents the computer program that was used to obtain the results described in this report. The added mass of the barge is calculated using Equation 24. A fourth-order Runge-Kutta technique is used to perform the numerical integrations over the bow and stern surfaces of the barge.

Note that the program uses a substitution for the function $1/\cosh(x)$, which occurs in the velocity potential function and its derivatives. Large argument in the $\cosh(x)$ function cause errors. The hyperbolic secant is actually desired, but FORTRAN does not include this function intrinsically. To avoid this problem, the trigonometric identity

$$\tanh^2(x) + \operatorname{sech}^2(x) = 1 \tag{A1}$$

is used to substitute for $1/\cosh(x)$, so that

$$\frac{1}{\cosh(x)} = \operatorname{sech}(x) = \sqrt{1 - \tanh^2(x)} \tag{A2}$$

Since $\tanh(x)$ is well behaved as x goes to infinity, this substitution makes the program much more reliable.

Use of the program is self-explanatory. Upon execution, it prompts the user for the necessary input defining the barge geometry and the test conditions. Modification of the dimensions of the barge requires modification of the computer code. The appropriate variables are annotated in the code.

```
        PROGRAM BargeAddMass
C   This program is used for the WES barge added-mass study.  There
C      are two barges of interest.  The first is the Jumbo Open-Hopper
C      Barge, 195 feet in length, and the Standard Open-Hopper Barge,
C      175 feet in length.  Only the Jumbo Barge will be considered
C      here.  The integrations for the added-mass will be done by
C      a fourth-order Runge-Kutta technique:
```

```
C                 INTEGRAL = deltaX/3 [f(X1) +4f(X2) +2f(X3) +4f(X4) ...
C                     ... +2f(Xn-1) +4f(Xn) +f(Xn+1) ]
      INTEGER j, k

      DOUBLE PRECISION pi, g, rho, degrees2rads
      DOUBLE PRECISION L, w, d, theta
      DOUBLE PRECISION alpha, h, u
      DOUBLE PRECISION beta
      DOUBLE PRECISION ya, yc, phi, a, b, c, x0, z, xa, xaprime, zeta,
     &    zetaprime
      DOUBLE PRECISION f1, f2, f3, f4, f1prime, f2prime, f3prime, phia
      DOUBLE PRECISION phiaprime, dphix, dphixprime, dphiz, dphizprime
      DOUBLE PRECISION fn(11), intz(21), integralA, integralC
      DOUBLE PRECISION mwbow, mwstern, mw

C     **********    Constants
      pi= 4.D0 *DATAN(1.D0)
      g= 32.2d0              ! ft/s^2
      rho= 62.4d0 /g         ! mass density of water
      degrees2rads= pi /180.D0  ! conversion factor: degrees to radians

C     **********    Barge data
      WRITE(*,*) 'Enter barge wetted length (ft)'
      READ(*,*) L
      WRITE(*,*) 'Enter barge wetted beam (ft)'
      READ(*,*) w
      WRITE(*,*) 'Enter barge draft (ft)'
      READ(*,*) d
      WRITE(*,*) 'Enter bow/stern rake angle (degrees)'
      READ(*,*) theta
      theta= theta *degrees2rads   ! bow/stern rake angle, rads

C     **********    Waterway data
      WRITE(*,*) 'Enter barge speed (ft/s)'
      READ(*,*) u
      WRITE(*,*) 'Enter water depth (ft)'
      READ(*,*) h
      WRITE(*,*) 'Enter distance from bow corner to wall (ft)'
      READ(*,*) ya
      WRITE(*,*) 'Enter angle of approach to wall (degrees)'
      READ(*,*) alpha
      alpha= alpha *degrees2rads   ! wall approach angle, rads

C     **********    The parametric coefficients in the analysis
C                     are as follows:
      yc= ya +L *DSIN(alpha)
      phi= 0.5673d0 *(pi +1.d0 /DTAN(theta) ) *u**3 /g
      a= u/ phi
      c= pi /h
```

```fortran
      b= DSQRT( DABS(-a*a +c*c) )
      beta= -b *w /2.d0
      x0= pi *u**2 /(2.d0*g)

C  NOTE: In the following, prime refers to the image barge

C  **********   Bow calculations:
      zeta= -w/2

C  Vertical iteration loop
      DO 10 j= 1, 21
        z= -d

C  Transverse iteration loop
        DO 20 k= 1, 11
          xa= x0 +z /DTAN(theta)
          xaprime= xa *( 2.d0 *DCOS(alpha) -1.d0) +
     &    w *DSIN(alpha) *DCOS(alpha) +2.d0 *ya *DSIN(alpha)
          zetaprime= zeta *( 2.d0 *DCOS(alpha) -1.d0) -
     &    xa *DSIN(2.D0*alpha) +w *(DCOS(alpha))**2 +
     &    2.d0 *ya *DCOS(alpha)
C          NOTE: In the below functions, the trigonometric substitution
C               1/COSH(x) = SECH(x) = SQRT(1 -(TANH(x))**2)
C          is used (which follows from the identity
C               (SECH(x))**2 +(TANH(x))**2 = 1
C          This is done because COSH(x) blows up as x becomes large.
          f1= DSQRT( 1.d0 -(DTANH(a *xa))**2 )
          f2= DTANH(a *xa)
          f3= 1.d0
          f4= DCOS(c*z)
          f1prime= DSQRT( 1.d0 -(DTANH(a *xaprime))**2 )
          f2prime= DTANH(a *xaprime)
          f3prime= DSQRT( 1.d0 -(DTANH(DABS(b *zetaprime) +beta))**2 )
          phia= -phi *f1 *f3 *f4
          phiaprime= -phi *f1prime *f3prime *f4
          dphix= a *phi *f1 *f2 *f3 *f4
          dphixprime= a *phi *f1prime *f2prime *f3prime *f4
          dphiz= c *phi *f1  *f3 *DSIN(c*z)
          dphizprime= c *phi *f1prime  *f3prime *DSIN(c*z)
          fn(k)= (phia +phiaprime) *( (dphix +dphixprime) *
     &    DSIN(theta) -(dphiz +dphizprime) *
     &       DCOS(theta)/DTAN(theta) )
          z= z+d /10.d0
20      CONTINUE

        intz(j)= (d/10.d0) *( fn(1) +4.d0*fn(2) +2.d0*fn(3) +
     &    4.d0*fn(4) +
     &    2.d0*fn(5) +4.d0*fn(6) +2.d0*fn(7) +4.d0*fn(8) +2.d0*fn(9) +
     &    4.d0*fn(10) +fn(11) )
```

```fortran
            zeta= zeta +w /20.d0
  10    CONTINUE

        integralA= (w/20.d0) *( intz(1) +4.*intz(2) +2.d0*intz(3) +
     &      4.d0*intz(4) +2.d0*intz(5) +4.d0*intz(6) +2.d0*intz(7) +
     &      4.d0*intz(8) +2.d0*intz(9) +
     &      4.d0*intz(10) +2.d0*intz(11) +4.d0*intz(12) +2.d0*intz(13) +
     &      4.d0*intz(14) +2.d0*intz(15) +4.d0*intz(16) +2.d0*intz(17) +
     &      4.d0*intz(18) +2.d0*intz(19) +4.d0*intz(20) +intz(21) )
        mwbow= DABS( rho *integralA /u**2 )

C       **********   Stern calculations:
        zeta= -w /2.d0

C       Vertical iteration loop
        DO 30 j= 1, 21
          z= -d

C       Transverse iteration loop
        DO 40 k= 1, 11
          xa= x0 +z /DTAN(theta)
          xaprime= xa *( 2.d0 *DCOS(alpha) -1.d0) +
     &      w *DSIN(alpha) *DCOS(alpha) +2.d0 *yc *DSIN(alpha)
          zetaprime= zeta *( 2.D0 *DCOS(alpha) -1.d0) -
     &      xa *DSIN(2.D0*alpha) +w *(DCOS(alpha))**2 +
     &      2.d0 *yc *DCOS(alpha)
C             NOTE: In the below functions, the trigonometric substitution
C                1/COSH(x) = SECH(x) = SQRT(1 -(TANH(x))**2)
C          is used (which follows from the identity
C                (SECH(x))**2 +(TANH(x))**2 = 1
C          This is done because COSH(x) blows up as x becomes large.
          f1= DSQRT( 1.d0 -(DTANH(a *xa))**2 )
          f2= DTANH(a *xa)
          f3= 1.d0
          f4= DCOS(c*z)
          f1prime= DSQRT( 1.d0 -(DTANH(a *xaprime))**2 )
          f2prime= DTANH(a *xaprime)
          f3prime= DSQRT( 1.d0 -(DTANH( DABS(b *zetaprime) +beta))**2 )
          phia= -phi *f1 *f3 *f4
          phiaprime= -phi *f1prime *f3prime *f4
          dphix= a *phi *f1 *f2 *f3 *f4
          dphixprime= a *phi *f1prime *f2prime *f3prime *f4
          dphiz= c *phi *f1 *f3 *DSIN(c*z)
          dphizprime= c *phi *f1prime *f3prime *DSIN(c*z)
          fn(k)= (phia +phiaprime) *( (dphix +dphixprime) *
     &      DSIN(theta) -(dphiz +dphizprime) *
     &        DCOS(theta)/DTAN(theta) )
          z= z+d /10.d0
  40    CONTINUE
```

```fortran
         intz(j)= (d/10.d0) *( fn(1) +4.d0*fn(2) +2.d0*fn(3) +4.d0*fn(4) +
     &     2.d0*fn(5) +4.d0*fn(6) +2.d0*fn(7) +4.d0*fn(8) +2.d0*fn(9) +
     &     4.d0*fn(10) +fn(11) )
         zeta= zeta +w/20.d0
  30  CONTINUE

         integralC= (w/20.d0) *( intz(1) +4.d0*intz(2) +2.d0*intz(3) +
     &       4.d0*intz(4) +
     &       2.d0*intz(5) +4.d0*intz(6) +2.d0*intz(7) +4.d0*intz(8) +
     &       2.d0*intz(9) +
     &       4.d0*intz(10) +2.d0*intz(11) +4.d0*intz(12) +2.d0*intz(13) +
     &       4.d0*intz(14) +2.d0*intz(15) +4.d0*intz(16) +2.d0*intz(17) +
     &       4.d0*intz(18) +2.d0*intz(19) +4.d0*intz(20) +intz(21) )
         mwstern= DABS( rho *integralC /u**2 )

         mw= mwbow +mwstern
         WRITE(*,*) 'Added weight =', mw *g /2000.d0, ' tons.'
         STOP
         END
```

Appendix B
Example Input and Output Runs

This appendix presents sample calculations using the computer code presented in Appendix A. Two sample cases are input, and the corresponding output is listed.

The first case is for the loaded JOHB abutting the wall at a right angle:

Enter barge wetted length (ft)
195.
Enter barge wetted beam (ft)
35.
Enter barge draft (ft)
10.
Enter bow/stern rake angle (degrees)
45.
Enter barge speed (ft/s)
3.
Enter water depth (ft)
18.
Enter distance from bow corner to wall (ft)
0.
Enter angle of approach to wall (degrees)
90.
Added weight =   3.07247498044177   tons.

The second case is for the loaded JOHB traveling parallel to the wall in open waters:

Enter barge wetted length (ft)
195.
Enter barge wetted beam (ft)
35.
Enter barge draft (ft)
10.

Enter bow/stern rake angle (degrees)
45.
Enter barge speed (ft/s)
3.
Enter water depth (ft)
18.
Enter distance from bow corner to wall (ft)
70.
Enter angle of approach to wall (degrees)
0.
Added weight = 3.14077173417141   tons.

REPORT DOCUMENTATION PAGE

1. REPORT DATE (DD-MM-YYYY)	2. REPORT TYPE	3. DATES COVERED (From - To)
November 2002	Final report	

4. TITLE AND SUBTITLE

Analysis of the Added Mass of a Barge in Restricted Waters; Phase 1 Model

5a. CONTRACT NUMBER

5b. GRANT NUMBER

5c. PROGRAM ELEMENT NUMBER

6. AUTHOR(S)

Michael E. McCormick, David R. B. Kraemer,
Patrick Hudson, William Noble

5d. PROJECT NUMBER

5e. TASK NUMBER

5f. WORK UNIT NUMBER
INP WU 33143

7. PERFORMING ORGANIZATION NAME(S) AND ADDRESS(ES)

The Johns Hopkins University, Department of Civil Engineering
3400 N. Charles Street, Baltimore, MD 21218-2686

8. PERFORMING ORGANIZATION REPORT NUMBER

9. SPONSORING / MONITORING AGENCY NAME(S) AND ADDRESS(ES)

U.S. Army Corps of Engineers, Washington, DC 20314-1000;
U.S. Army Engineer Research and Development Center
Information Technology Laboratory, 3909 Halls Ferry Road
Vicksburg, MS 39180-6199

10. SPONSOR/MONITOR'S ACRONYM(S)

11. SPONSOR/MONITOR'S REPORT NUMBER(S)

ERDC/ITL TR-02-8

12. DISTRIBUTION / AVAILABILITY STATEMENT

Approved for public release; distribution is unlimited.

13. SUPPLEMENTARY NOTES

14. ABSTRACT

This report presents a theoretical analysis of the added mass of barges in restricted waters. The added mass behaviors with varying waterway and barge parameters are predicted. While variations in both the water depth and barge speed are seen to strongly influence the added-mass (added-weight) values, the separation between the barge and quay (side) wall is seen to have influence near the wall. For practical cases where the barge has rake angles less than 90 deg, the wall effect is evident only when the barge motion is parallel or nearly parallel to the wall. This analysis, based partly on empirical observations, proves useful for the initial investigation of the problem.

Described herein is a low-speed analysis. That is, the current analysis is based on an observed free-surface phenomenon that occurs only at slow speeds. The barge speed range is between 0 and 4 fps (0 and 1.2 m/s). At higher speeds, the surface waves system becomes a subcritical ship wave system, having transverse and divergent component waves. The higher speeds will be analyzed in the follow-on part (Phase 2) of this research. In that study, the boundary-element technique will be applied to the problem.

15. SUBJECT TERMS

Added mass	Potential theory	Wall effect
Image technique	Ship waves	

16. SECURITY CLASSIFICATION OF:

a. REPORT	b. ABSTRACT	c. THIS PAGE	17. LIMITATION OF ABSTRACT	18. NUMBER OF PAGES	19a. NAME OF RESPONSIBLE PERSON
UNCLASSIFIED	UNCLASSIFIED	UNCLASSIFIED		37	19b. TELEPHONE NUMBER (include area code)